Chapter

Combination of the CEEM Decomposition with Adaptive Noise and Periodogram Technique for ECG Signals Analysis

Azzedine Dliou, Samir Elouaham, Rachid Latif and Mostafa Laaboubi

Abstract

The electrocardiogram (ECG) signal is a fundamental tool for patient treatment, especially in the cardiology domain, due to the high mortality rate of heart diseases. The main objective of this paper is to present the most optimal techniques that can link the processing and analysis of ECG signals. This work is divided into two steps. In the first one, we propose a comparison between some denoising techniques that can reduce noise affecting the ECG signals; these techniques are the empirical mode decomposition (EMD), the ensemble empirical mode decomposition (EEMD), and the complete ensemble empirical mode decomposition with adaptive noise (CEEMDAN). In the second one, we make a comparison of three time-frequency techniques: the Choi-Williams (CW), the periodogram (PE), and the smoothed pseudo Wigner-Ville (SPWV). Firstly, the obtained results illustrate the effectiveness of the CEEMDAN in reducing noise that interferes with ECG signals compared to other denoising methods. Secondly, they show that the periodogram time-frequency technique gives a good detection and localization of the main components in the time-frequency plan of ECG signals. This work proves the utility of the combination of the periodogram and CEEMDAN techniques in analyzing the ECG signals.

Keywords: ECG, CEEMDAN, periodogram, time-frequency, denoising

1. Introduction

The heart function can be obtained by storing the voltage variations which occur on some parts of the human body surface [1–3]. The electrocardiogram (ECG) is the record of those voltage variations over time. This biomedical signal presents a fundamental tool used in cardiology to detect cardiac diseases. The normal ECG signal is characterized by a sequence of some well-defined components as P wave, QRS complex, and T wave [1–3]. ECG signals are most of the time contaminated by different noise sources, like power-line interference, baseline wander, muscle noise and motion artifact, and other noises, which in different cases make the

identification of standard ECG features very difficult and lead to a misjudgment of patient diagnostic [4]. Consequently, to deal with this problem, a task of removing noise from ECG signal, as preprocessing step, has become very important.

To tackle this problem, the first part of the current work proposes a comparison study of the following denoising methods, empirical mode decomposition (EMD), ensemble empirical mode decomposition (EEMD), and complete ensemble empirical mode decomposition with adaptive noise (CEEMDAN), to define which one gives the best results in the case of the normal and abnormal ECG signals.

Huang et al. [5] have introduced the empirical mode decomposition (EMD) method to analyze nonstationary and nonlinear signals. The EMD major advantage is that the basic functions are derived from the signal itself; however, the EMD process presents a mode mixing. To surmount this problem, we resort to ensemble empirical mode decomposition (EEMD); this denoising method employs EMD to integrated signals with white Gaussian noise [6]. Even so, signals with added noise can produce a large number of iterations in the EEMD process, and signal result holds residual noise after decomposition. These downsides are resolved with a variant denoising method, called CEEMDAN; this technique achieves an accurate original signal reconstruction. The CEEMDAN iteration number is minus than half of the EEMD iteration number [7].

Traditionally, ECG signal, are analyzed in the time domain by skilled physicians. However, detecting pathological conditions in the time domain is not always evident [8]. The precision and the exactitude of the diagnosis are in relation with the cardiologist experience and the concentration rate.

This fact has incentive applying the frequency domain techniques, such as Fourier transform (FT) analysis [9]. The development of the Cooley-Tukey algorithm made Fourier techniques widely available; this algorithm allows the use of the computation more efficient [10]. However, the ECG signals are multicomponent nonstationary signals [8]; accurate time-varying spectral estimates can be extremely difficult to obtain with Fourier techniques which give only globally averaged information.

To overcome this problem, time-frequency techniques can be a good solution. These techniques can reveal the multicomponent nature of such signals and how the signal spectrum evolves over time [11–13].

Time-frequency techniques can be classified into two major categories: parametric and nonparametric techniques. Nonparametric time-frequency techniques present a good solution for analyzing multicomponent nonstationary signal [13–15]. However, these techniques suffer from the presence of cross-terms [16–18], which can hide the interesting signal information. A lot of efforts have been made to select the best time-frequency technique which provides a low degree of cross-term effect [13–18].

The second part of the this work is consecrated to compare three time-frequency techniques, Choi-Williams (CW), periodogram (PE), and smoothed pseudo Wigner-Ville (SPWV), to deliver which one furnishes the best results in analysis terms of this type of biomedical signals.

The signals that will be the subject of this comparative study are extracted from [19]. These signals are chosen with different pathologies and variant forms in order to make the study more credible.

This paper is organized as follows: the "Theoretical background" section is dedicated to present the chosen denoising methods, the three time-frequency techniques, and the selected ECG signals. For a qualitative performance, comparison of the denoising methods and the time-frequency techniques is performed in the "Results and discussion" section, accompanied with a discussion of the obtained results. Finally, this study is concluded with a "Conclusion" section.

2. Theory background

2.1 Denoising techniques used

2.1.1 Empirical mode decomposition (EMD)

Huang et al. had defined a tool named EMD to decompose adaptively a signal in a set of AM-FM components [5]. No mathematical foundations or analytical expressions have been proposed for the technique theoretical study. In various domains, such as biomedicine, acoustics, seismology, or study of climate phenomena, the EMD has been used successfully in several works to treat real data [20, 21]. These studies had provided satisfaction and good results in signal processing, especially for nonstationary ones. A nonstationary signal is decomposed adaptively by the EMD technique into a sum of functions oscillatory band-limited d(t). These functions, called intrinsic mode functions $IMF_J(t)$, oscillate around zero. The intrinsic mode functions can express the signal x(t) by the following expression:

$$x(t) = \sum_{j=1}^{k} d_j(t) + r(t) \tag{1}$$

where r(t) is the low-frequency residue.
Two conditions must be satisfied by each $IMF_J(t)$:

- The zero crossings and extreme signal numbers must be equal all over the analyzed signal.

- The envelope average defined by signal local extreme must be equal to 0 at any point. On the one hand, the low-oscillation components are represented by the higher-order $IMF_J(t)$, and on the other hand, the fast ones are presented by lower-order $IMF_J(t)$. The $IMF_J(t)$ number is variable for different decomposed signals and depends on the signal spectral content. The technical aspects of the EMD implementation are decomposed on five steps given by the following algorithm [5]:

Step 1: Extraction of the signal x(t) extreme.
Step 2: By the maximum interpolation (resp. minima), an upper envelope $e_{max}(t)$ (resp. lower $e_{min}(t)$) is deduced.
Step 3: The half envelope sum is defined as a local average m(t) by the following expression:

$$m(t) = (e_{\max}(t) + e_{\min}(t))/2 \tag{2}$$

Step 4: Deduction of $d_J(t) = IMF_J(t)$, a local detail by

$$d(t) = x(t) - m(t) \tag{3}$$

Step 5: The expression (1) gives the iteration.
The high frequency terms are contained in the first IMF, which also involves the following terms of decreasing frequency up to forwarding only a low-frequency residue.

2.1.2 Ensemble empirical mode decomposition (EEMD)

The ensemble empirical mode decomposition (EEMD) method was proposed to surpass the mode mixing disadvantage which exists in EMD technique [22]. By repeating the processes of decomposition, the EMD provides all solutions giving the true IMF.

The following steps give the EEMD method algorithm:

Step 1: The analyzed signal is added with a predefined amplitude white noise.

Step 2: The resulted signal is decomposed by using the EMD method.

Step 3: The above signal decomposition is repeated with different fixed amplitude white noises.

Step 4: Calculation of the final results is equal to the ensemble means of the decomposition results.

As finite number of intrinsic mode functions (IMFs) and a residue, the signal x (k) is decomposed:

$$x(k) = \sum_{i=1}^{n} \widehat{c}_i + \widehat{r} \tag{4}$$

where n defines the IMF number, $\widehat{c}_i$ is the i-th IMF which is the corresponding IMF ensemble mean resulted from all of the decomposition processes, and $\widehat{r}$ is the residue mean obtained from all processes of the decomposition.

2.1.3 Complete ensemble empirical mode decomposition with adaptive noise (CEEMDAN)

2.1.3.1 CEEMD algorithm

Although the mode mixing effect is mitigated by the EEMD method, if the ensemble number is small, some noise will continue to exist in the corresponding IMF(s). To deal with this problem and assure a noise-free IMF, a CEEMD algorithm [7–23] is defined by the following steps:

Step 1: The target signal x(t) is added by positive and negative white noise $\varepsilon^{+,-}(t)$ in order to create two new signals $x^{+}(t)$ and $x^{-}(t)$:

$$\begin{aligned} x^{+}(t) &= x(t) + \varepsilon^{+}(t) \\ x^{-}(t) &= x(t) + \varepsilon^{-}(t) \end{aligned} \tag{5}$$

Step 2: Step 1 is repeated, and by using the EMD algorithm, each of the new signals $x^{+}(t)$ and $x^{-}(t)$ is decomposed.

Step 3: For the $x^{+}(t)$ and $x^{-}(t)$ data sets, two IMF sets are obtained; (4) by averaging the IMF_k^i in Eq. (11), the decomposed result is calculated, where IMF_k^i defines the i-th IMF of the k-th iteration;

$$\overline{IMF}_1(n) = \frac{1}{I} \sum_{i=1}^{l} \overline{IMF_k^i}(n) \tag{6}$$

2.1.3.2 Complete ensemble empirical mode of decomposition with adaptive noise (CEEMDAN)

On the one hand, using EEMD overcomes the EMD mode mixing problem, but on the other hand, this technique presents a problem. The number of iterations

required in EEMD process is higher, added to the residual noise remaining in the reconstructed signal. So we have a new method called CEEMD; this technique provides an exact reconstruction of the original signal and gives better separation of modes with low computation cost. In this method the first mode $\overline{\mathrm{IMF}}_1(\mathrm{n})$ is obtained in the same way as in EEMD. It's computed over an ensemble of $\mathrm{r}_1(\mathrm{n})$ plus different realizations of a given noise obtaining $\overline{\mathrm{IMF}}_2(\mathrm{n})$ by averaging. Here $\mathrm{E_j}$ [.] operator provides j^{th} mode obtained by EMD. w^{i} is the white noise [7–24].

The steps of CEEMDAN decomposition are as follows:

Step 1: Decompose $\mathrm{x(n)} + \varepsilon_0 \mathrm{w_i(n)}$ to obtain the first mode by using:

$$\overline{IMF}_1(n) = \frac{1}{I}\sum_{i=1}^{l}\overline{IMF_k^i}(n) \tag{7}$$

where w_0 is the added white noise amplitude and $\varepsilon(t)$ is the white noise with unit variance.

Step 2: Compute the difference signal:

$$r_1(n) = x(n) - \overline{IMF}_1(n) \tag{8}$$

Step 3: Decompose $r_1(n) + w_1 E_1\left(\varepsilon^i(n)\right)$, to obtain the first mode, and define the second mode by

$$\overline{IMF}_2(n) = \frac{1}{I}\sum_{i=1}^{l} E_1\left(r_1(n) + w_1 E_1\left(\varepsilon^i(n)\right)\right) \tag{9}$$

For k = 2, ..., K, calculate the k-th residue and obtain the first mode. Define the (k + 1)-th mode as follows:

$$\overline{IMF}_{k+1}(n) = \frac{1}{I}\sum_{i=1}^{l} E_1\left(r_k(n) + w_k E_k\left(\varepsilon^i(n)\right)\right) \tag{10}$$

where E_1 is a function to extract the j^{th} IMF decomposed by EMD.

Step 4: Continue this process until residue is no longer feasible. Final residue

$$R(n) = x(n) - \sum_{k=1}^{k}\overline{IMF}_k \tag{11}$$

So the given signal can be expressed as

$$x(n) = R(n) + \sum_{k=1}^{k}\overline{IMF}_k \tag{12}$$

A quantitatively comparison of these three filtering methods' performance will be made based on two metrics: mean square error (MSE) and percent root mean square difference (PRD). The MSE and PRD are used to evaluate the quality of the information which is preserved in the denoised ECG signal. The MSE and the PRD are computed as follows:

$$MSE = \frac{1}{N}\sum_{n=1}^{N}\left(x(n) - \overline{x}(n)\right)^2 \tag{13}$$

$$PRD = \sqrt{\frac{\sum_{n=1}^{N}(x(n) - \overline{x}(n))^2}{\sum_{n=1}^{N}x^2(n)}} * 100 \tag{14}$$

where x(n) is the original ECG signal, $\overline{x}(n)$ denotes the reconstruction of the ECG signal, and N is the number of ECG samples used.

2.2 Time-frequency techniques

In time-varying spectral analysis, time-frequency techniques have found a large number of application [8–15]. There is no single time-frequency representation due to the signal energy distribution which joints time and frequency coordinates. There are many time-frequency techniques and many ways to define them. The most popular time-frequency representation class is called the quadratic or Cohen (1989) class. The Choi-Williams (CW), the periodgram (PE), and the smoothed pseudo Wigner-Ville (SPWV) techniques were chosen from the different time-frequency techniques belonging to this representation time-frequency set, due to its interesting properties.

2.2.1 Choi-Williams distribution (CWD)

The Choi-Williams distribution CWD(t, f) was a significant step in the field of time-frequency analysis where it opened the way for optimizing resolution with cross-term reduction [25]:

$$CWD_x(t,f) = \frac{1}{4\pi^2}\int_{-\infty}^{\infty}\int\int_{-\infty}^{+\infty}\exp^{-j\theta t - j\tau\omega + j\theta u}\phi(\theta,\tau)A_u du d\tau d\theta \tag{15}$$

where

$$A_u = x\left(u + \frac{\tau}{2}\right)x^*\left(u - \frac{\tau}{2}\right) \tag{16}$$

and $\phi(\theta,\tau) = e^{\frac{\theta^2\tau^2}{\sigma}}$.

The smoothing of the distribution is controlled by the constant σ. If $\sigma \to \infty$, the Choi-Williams distribution (CWD) will simply converge to the Wigner-Ville distribution, as the kernel goes to 1.

2.2.2 Periodogram technique

The minimum variance estimator, named Capon estimator (CA), does not fix a model on the signal. At each frequency f, this method seeks a matched filter whose response is 1 for the frequency f and 0 everywhere else [26]:

$$CA(t,f) = a(n,f)^H R_x a(t,f) = \frac{1}{Z_f^H . R_x[t]^{-1} . Z_f} \tag{17}$$

where CA(n, f) means the filter Capon output power. By the discrete signal x(n) sampled at the period t_e, this filter is excited; a(n, f) = (a_0, ..., a_p) is the filter impulse response at frequency n; $R_x[n] = E\{x[n]x^T[n]\}$ is the crossed x(n) autocorrelation matrix of dimension (p + 1)*(p + 1); x[n] = (x(n − p), ..., x(n)) is the selected signal at time n; $Z^H{}_f$ (1, $e^{2i\pi ft}{}_e$, ..., $e^{2i\pi ft}{}_e{}^p$) is the steering vector; (p + 1) is

the number of filter coefficient and the exponent H for conjugate transpose and the superscript T for transpose.

The periodogram (PE) is the derivate of the Capon (CA) technique. The spectral estimator of this method is defined by the following equation [26]:

$$PE(t,f) = Z_f^H . R_x . Z_f / \left((\mathrm{p}+1)^2 \right) \tag{18}$$

By sliding windows, the PE technique can be used. Theoretical criterion does not exist for selecting window duration and filter order. The parametric technique frequency response presents different properties according to the signal characteristics. The time-frequency resolution depends principally of the window choice. Usually, the PE estimator gives a better frequency resolution.

2.2.3 Smoothed pseudo Wigner-Ville technique (SPWV)

The Cohen class exhibits most nonparametric time-frequency techniques [16, 17]. The smoothed pseudo Wigner-Ville technique belongs in particular to this class [16, 17]. To overcome the major weakness of the Wigner-Ville time-frequency representation, which is the covering of frequential components, the SPWV has been proposed between the different existing nonparametric time-frequency techniques; for that, the analytical signal $x_a(t)$ replaces the real signal x(t). The following expression defines this signal:

$$x_a(t) = x(t) + iH\{x(t)\} \tag{19}$$

where $i^2 = -1$, H{x(t)} is the Hilbert transform of the signal with real values, x(t).

Expression (20) defines the analytical signal $x_a(t)$ spectrum, $F_a(k)$:

$$F_a(k) = \begin{cases} 2X(k) & if\ 0 < k < N/2 \\ X(0) & if\ k = 0,\ \ N/2 \\ 0 & if\ N/2 < k < N \end{cases} \tag{20}$$

where X(k) represents the original signal x(t) Fourier transform and N is the point number.

The function $W_x(t, f)$ is the Wigner-Ville distribution related to a signal x(t), of finished energy. This distribution depends on the temporal (t) and frequential (f) parameters. The following expression defines this distribution [16, 17]:

$$W_{x_a}(t,f) = \int_{-\infty}^{+\infty} x_a\left(t + \frac{\tau}{2}\right) . x^*{}_a\left(t - \frac{\tau}{2}\right) e^{-2i\pi f \tau} d\tau \tag{21}$$

where $x^*{}_a(t)$ indicates the complex conjugate of $x_a(t)$.

The SPWV is used principally to decrease the problem of the interference terms happening between the inner components that existed in Wigner-Ville image. The time-frequency image visibility is reduced by these terms [13, 14]. The SPWV technique is applied by using two smoothing windows h(t) and g(t). The utility of these smoothing windows entered into the definition of the Wigner-Ville technique is to guarantee an interference separate control both in time (g) and in frequency (h). This representation is defined by the following expression [16, 17]:

$$SPWV_x(t,f) = \int_{-\infty}^{+\infty} h\left|\left(\frac{\tau}{2}\right)^2\right| \int_{-\infty}^{+\infty} g(t-u)x_a\left(u+\frac{\tau}{2}\right) x_a^*\left(u-\frac{\tau}{2}\right) e^{-2i\pi f\tau} d\tau du \quad (22)$$

where h(t) is a smoothing frequential window and g(t) is a smoothing temporal window.

We compare also the performance of these three time-frequency techniques by using the same metrics that were used in the filtering method comparison.

2.3 Biomedical signals

Electrocardiogram signals allow to represent the human heart state. ECG signal is a fundamental tool commonly used in the heart medical domain to treat patients suffering from cardiac diseases. By measuring the potential difference between electrodes posed in well-known places in the patient skin, these signals are usually obtained. The ECG signal can be single channel or multichannel depending on how many electrodes are used, one or several. Important knowledge is obtained by cardiologists about the patient's heart function only by analyzing a minute feature of these signals.

The ECG signal has a well-defined P, QRS, and T signatures that represent each heartbeat. The duration, shape, and amplitude of these waves are considered as major features in time domain analysis.

Changes in the normal rhythmicity of a human heart may result in different cardiac arrhythmias, which may be immediately fatal or cause irreparable damage to the heart when sustained over a long period of time.

The following subsections present the different normal and abnormal ECG signals chosen for this study. These data were obtained from [19].

2.3.1 Normal ECG

Figure 1 shows the time domain of a normal ECG signal. The sampling frequency for this normal ECG signal was 128 samples/s and the signal length 8 s.

2.3.2 Atrial fibrillation ECG

Figure 2 shows a length of 4 s of an abnormal atrial fibrillation ECG signal obtained from a patient with malignant ventricular arrhythmia. The sampling frequency for this signal was 250 samples/s.

The atrial rate exceeds 350 beats per minute in this type of arrhythmias. This arrhythmia occurs due to an uncoordinated activation and contraction of different parts of the atrial which leads to ineffective pumping of blood into the ventricles.

2.3.3 Ventricular tachyarrhythmia ECG

Figure 3 shows a length of 4 s of a ventricular tachyarrhythmia ECG signal with a 250 samples/s sampling frequency.

This abnormal signal presents a misalignment of the third QRS complex.

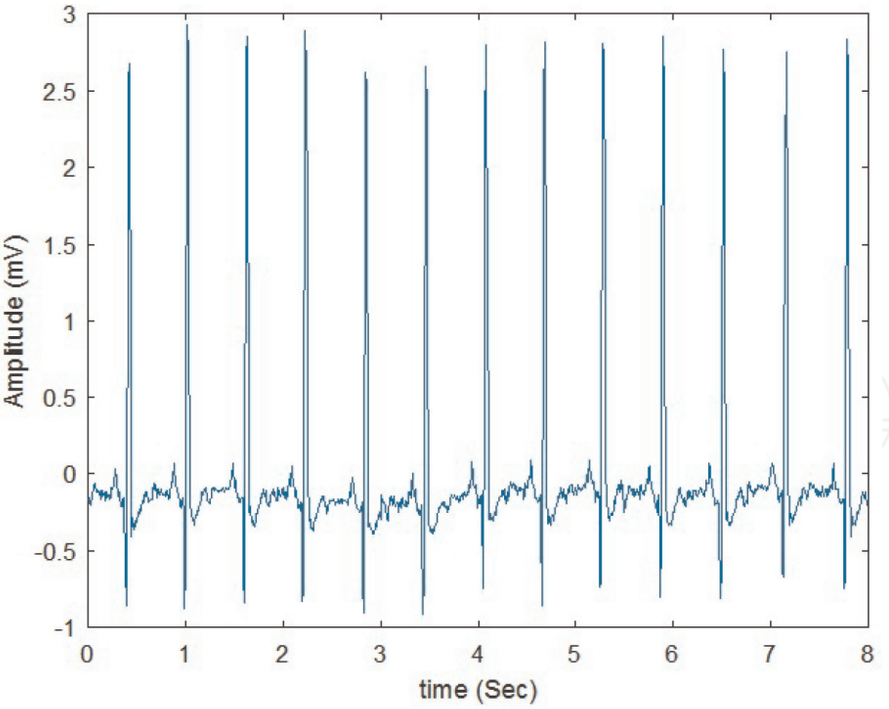

Figure 1.
Normal ECG signal.

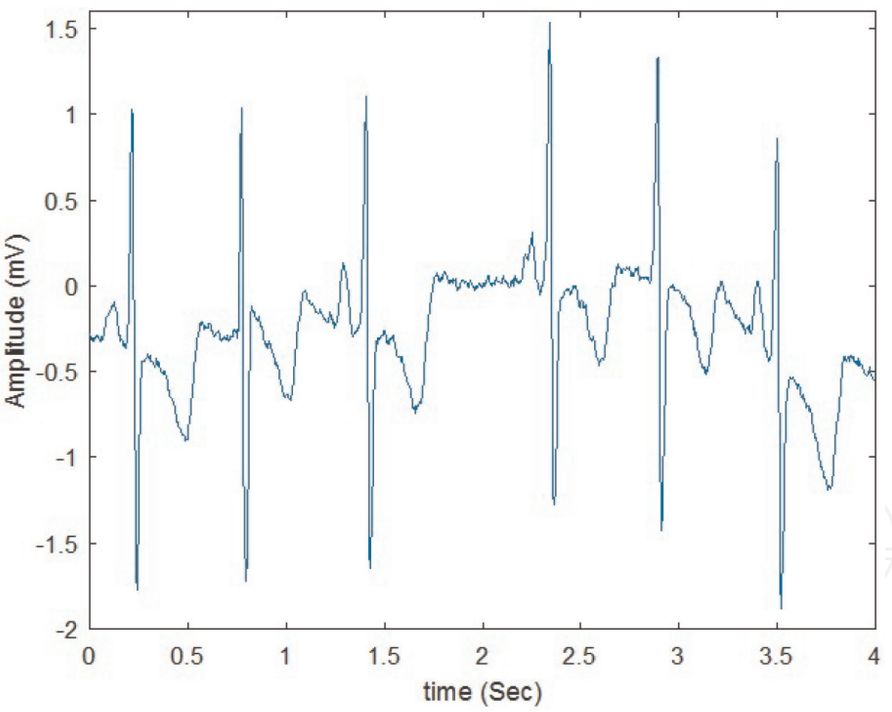

Figure 2.
Atrial fibrillation ECG signal.

2.3.4 Malignant ventricular arrhythmia ECG

Figure 4 shows a length of 4 s of the time domain ECG signal obtained from a patient with malignant ventricular arrhythmia. The sampling frequency for this signal was 250 samples/s. The depolarization wave spreads through the ventricles by an irregular and therefore slower pathway. The QRS complex is thus wide and abnormal. Repolarization pathways are also different, causing the T wave to have an unusual morphology.

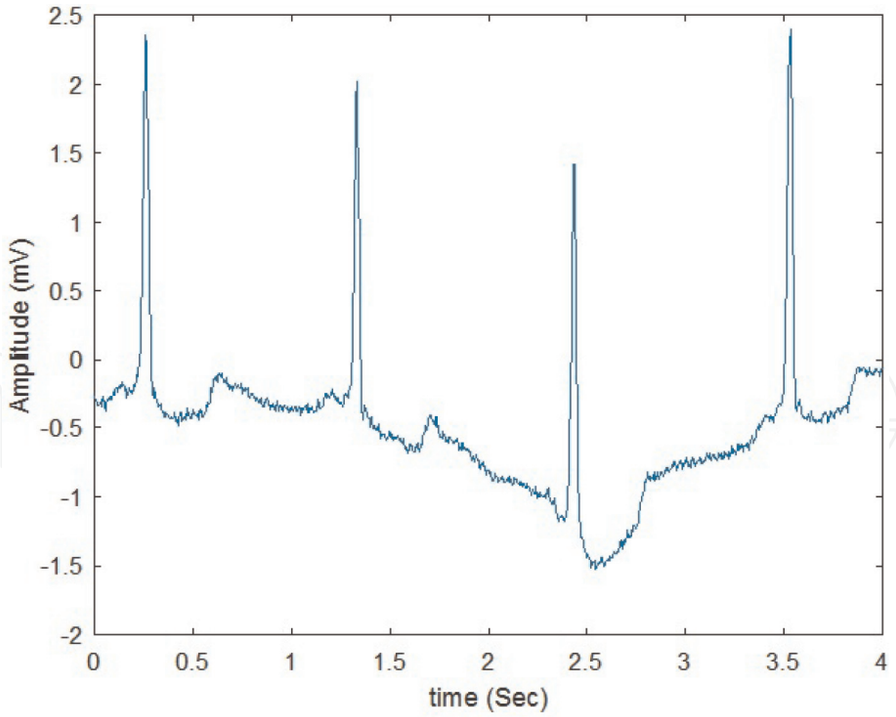

Figure 3.
Ventricular tachyarrhythmia ECG signal.

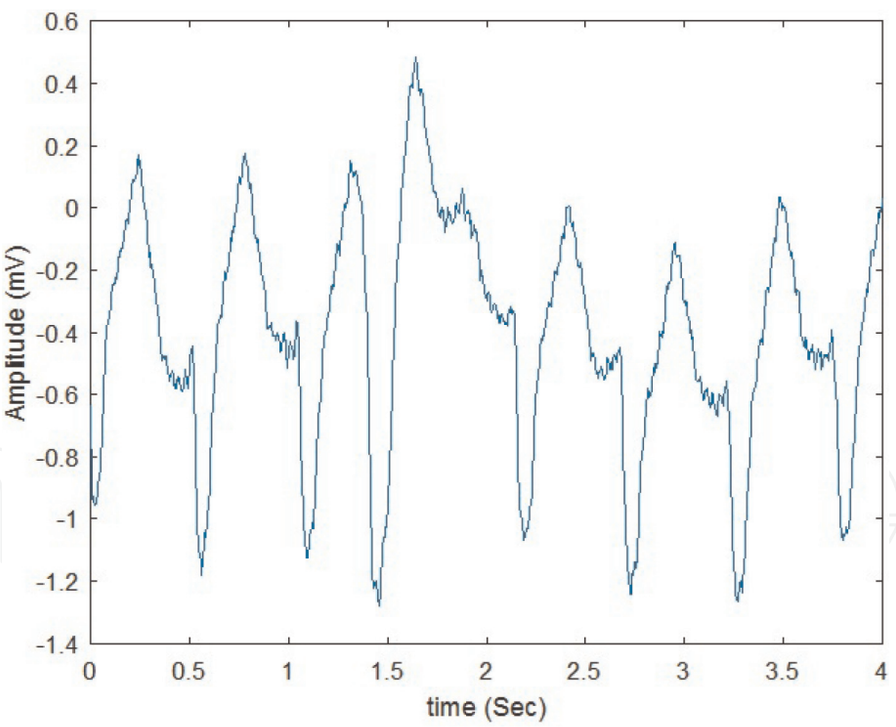

Figure 4.
Malignant ventricular arrhythmia ECG signal.

2.3.5 Supraventricular ECG

Figure 5 shows the time domain ECG signal of a patient with supraventricular arrhythmia. The sampling frequency for this abnormal ECG signal was 128 samples/s and the signal length 8 s. The shape of the QRS complex in this signal is abnormal at the QR part.

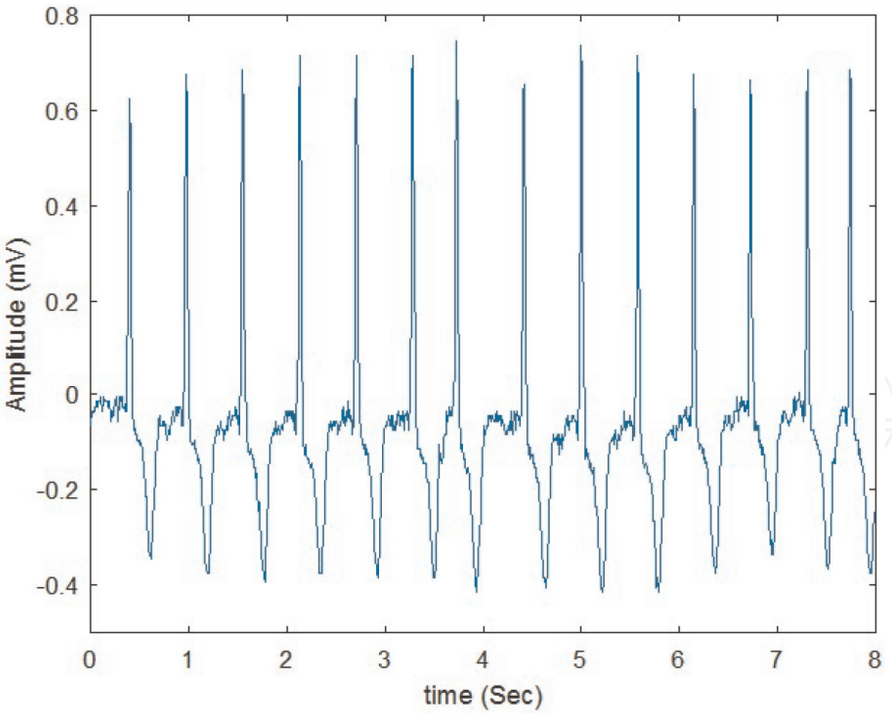

Figure 5.
Supraventricular arrhythmia ECG signal.

These normal and abnormal ECG signals were corrupted with noise CN generated by the following Eq. [4]:

$$CN = \frac{wbw * BW + wem * EM + wma * MA}{wbw + wem + wma} \tag{23}$$

where BW is the baseline wander noise, EM is the electromyogram noise, and MA is the motion artifact. Wbw, wem, and wma define the added noise percentage of baseline wander, electromyogram noise, and motion artifact noises, respectively. These parameters have been chosen with the following values wbw = 2, wem = 2, and wma = 5, which signified that the predominant noise in the noisy ECG signal is the motion artifact.

3. Results and discussion

3.1 Denoising methods

To evaluate the performance of the three denoising methods, EMD, EEMD, and CEEMDAN, a set of normal and abnormal ECG signals with different shapes were chosen. Before applying the proposed denoising methods, the ECG signals were corrupted with different values of signal-to-noise ratio (SNR); these values are from −5 dB to 20 dB with a 5 dB step.

Tables 1–5 report the performance of the denoising methods for the five ECG recordings. These tables present the obtained results of the mean square error (MSE), the root mean square error (RMSE), and the percent root mean square difference (PRD) for the following ECG signals, respectively, a normal ECG, an atrial fibrillation ECG, a ventricular tachyarrhythmia ECG, a malignant ventricular arrhythmia ECG, and a supraventricular arrhythmia ECG.

Figures 6–10 present the RMSE comparison graphs of the results obtained by using different denoising methods (EMD, EEMD, and CEEMDAN) to the five

SNR	EMD			EEMD			CEEMDAN		
	MSE	RMSE	PRD	MSE	RMSE	PRD	MSE	RMSE	PRD
−5	1.179	1.086	192.033	1.011	1.006	177.847	1.047	1.023	180.914
0	0.450	0.671	118.580	0.320	0.565	99.966	0.357	0.597	105.620
5	0.227	0.476	84.191	0.101	0.318	56.303	0.136	0.368	65.094
10	0.136	0.368	65.104	0.032	0.180	31.820	0.064	0.253	44.812
15	0.055	0.235	41.628	0.010	0.101	17.900	0.042	0.205	36.252
20	0.038	0.196	34.604	0.003	0.059	10.359	0.034	0.185	32.695

Table 1.
MSE, RMSE, and PRD of the normal ECG signal.

SNR	EMD			EEMD			CEEMDAN		
	MSE	RMSE	PRD	MSE	RMSE	PRD	MSE	RMSE	PRD
−5	0.780	0.883	179.314	0.768	0.877	177.928	0.767	0.876	177.727
0	0.254	0.504	102.241	0.243	0.493	100.025	0.243	0.493	100.150
5	0.097	0.311	63.129	0.077	0.277	56.300	0.078	0.280	56.837
10	0.042	0.204	41.404	0.025	0.157	31.797	0.026	0.163	33.003
15	0.023	0.153	31.050	0.008	0.087	17.760	0.010	0.099	20.117
20	0.017	0.132	26.796	0.003	0.051	10.373	0.005	0.070	14.131

Table 2.
MSE, RMSE, and PRD of the atrial fibrillation ECG signal.

SNR	EMD			EEMD			CEEMDAN		
	MSE	RMSE	PRD	MSE	RMSE	PRD	MSE	RMSE	PRD
−5	1.590	1.261	177.669	1.590	1.261	177.694	1.589	1.261	177.640
0	0.513	0.716	100.957	0.505	0.711	100.173	0.503	0.709	99.905
5	0.173	0.416	58.550	0.159	0.399	56.224	0.159	0.399	56.195
10	0.057	0.240	33.782	0.051	0.225	31.769	0.050	0.224	31.618
15	0.029	0.169	23.884	0.016	0.127	17.906	0.016	0.127	17.863
20	0.016	0.126	17.685	0.005	0.074	10.403	0.005	0.072	10.151

Table 3.
MSE, RMSE, and PRD of the ventricular tachyarrhythmia ECG signal.

considered ECG signals: normal ECG, atrial fibrillation ECG, ventricular tachyarrhythmia ECG, malignant ventricular arrhythmia ECG, and supraventricular arrhythmia ECG, respectively, at a SNR interval varying from −5 to 20 dB.

Figures 11–15 are presenting the obtained PRD results of the three denoising methods (EMD, EEMD, and CEEMDAN) to all the chosen ECG signals, normal ECG, atrial fibrillation ECG, ventricular tachyarrhythmia ECG, malignant ventricular arrhythmia ECG, and supraventricular arrhythmia ECG, respectively, at a SNR interval varying from −5 to 20 dB.

3.2 Time-frequency techniques

To compare the performance of the three chosen time-frequency techniques, Choi-Williams (CW), periodogram (PE), and smoothed pseudo Wigner-Ville (SPWV), we applied these time-frequency methods to ECG signals presented in

SNR	EMD			EEMD			CEEMDAN		
	MSE	RMSE	PRD	MSE	RMSE	PRD	MSE	RMSE	PRD
−5	0.918	0.958	177.481	0.922	0.960	177.902	0.920	0.959	177.673
0	0.291	0.539	99.900	0.291	0.540	99.946	0.291	0.539	99.921
5	0.092	0.303	56.142	0.092	0.304	56.221	0.092	0.303	56.214
10	0.029	0.171	31.672	0.029	0.171	31.692	0.029	0.171	31.628
15	0.009	0.096	17.863	0.009	0.096	17.856	0.009	0.096	17.846
20	0.003	0.056	10.291	0.003	0.055	10.214	0.003	0.055	10.122

Table 4.
MSE, RMSE, and PRD of the malignant ventricular arrhythmia ECG signal.

SNR	EMD			EEMD			CEEMDAN		
	MSE	RMSE	PRD	MSE	RMSE	PRD	MSE	RMSE	PRD
−5	0.137	0.370	179.290	0.135	0.367	177.814	0.135	0.367	177.867
0	0.047	0.217	105.004	0.043	0.206	99.982	0.043	0.207	100.557
5	0.017	0.131	63.466	0.013	0.116	56.276	0.014	0.119	57.717
10	0.008	0.090	43.633	0.004	0.066	31.748	0.005	0.071	34.536
15	0.006	0.079	38.091	0.001	0.037	18.000	0.002	0.047	22.774
20	0.004	0.061	29.538	0.0005	0.021	10.400	0.001	0.037	17.705

Table 5.
MSE, RMSE, and PRD of the supraventricular arrhythmia ECG signal.

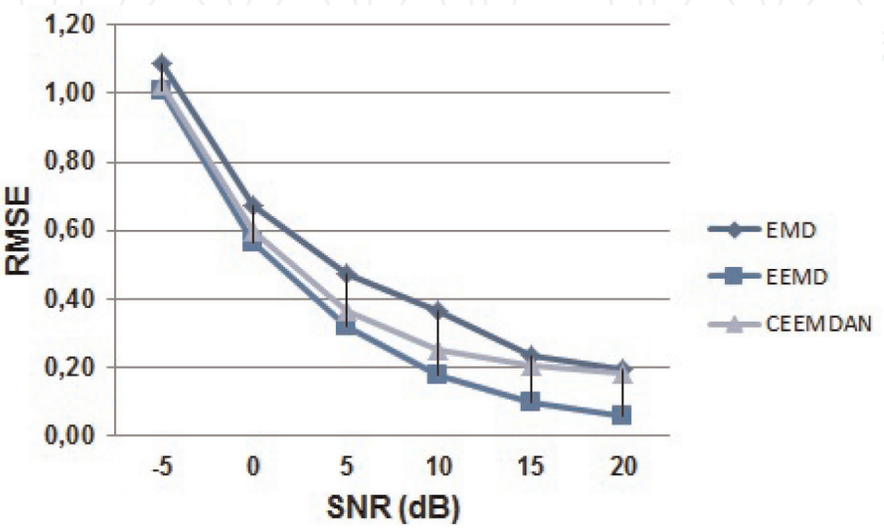

Figure 6.
RMSE comparison of the three denoising methods at different SNR levels for the normal ECG signal.

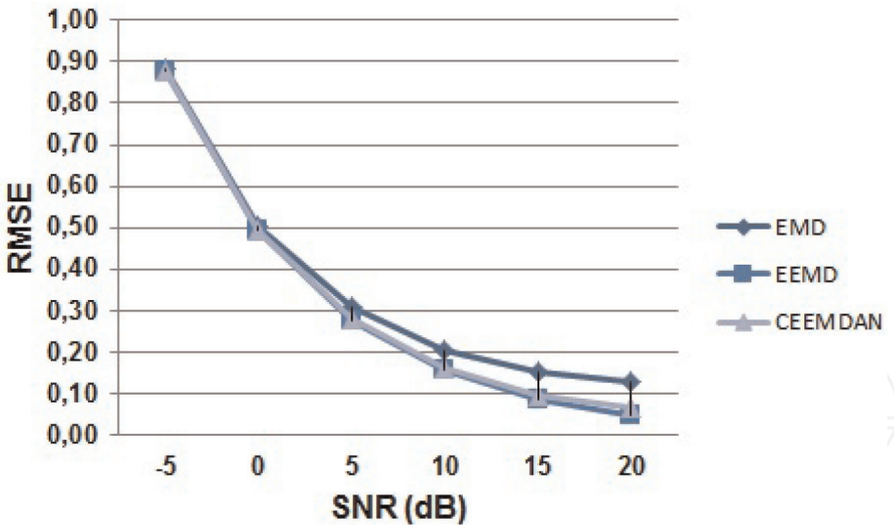

Figure 7.
RMSE comparison of the three denoising methods at different SNR levels for the atrial fibrillation ECG signal.

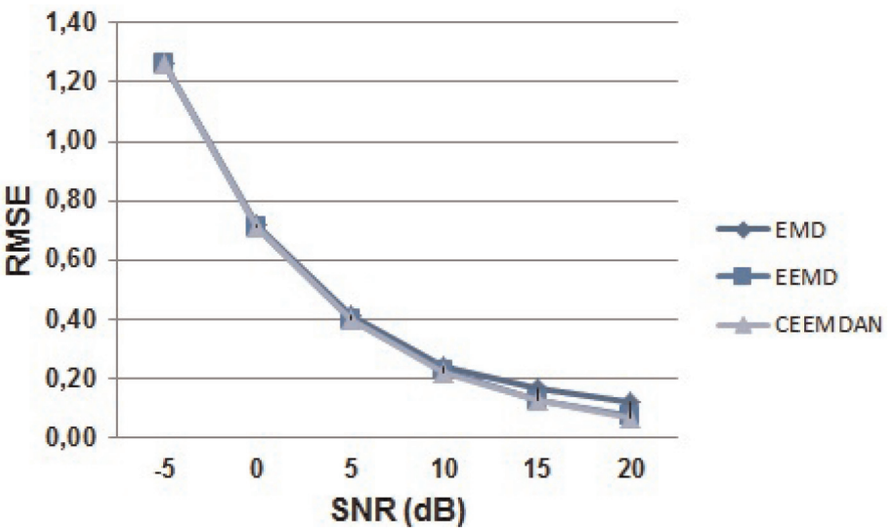

Figure 8.
RMSE comparison of the three denoising methods at different SNR levels for the ventricular tachyarrhythmia ECG signal.

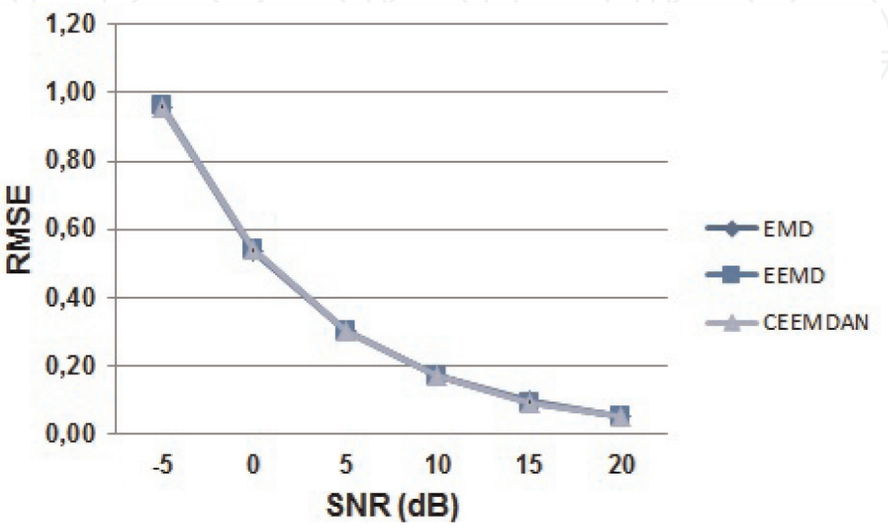

Figure 9.
RMSE comparison of the three denoising methods at different SNR levels for the malignant ventricular arrhythmia ECG signal.

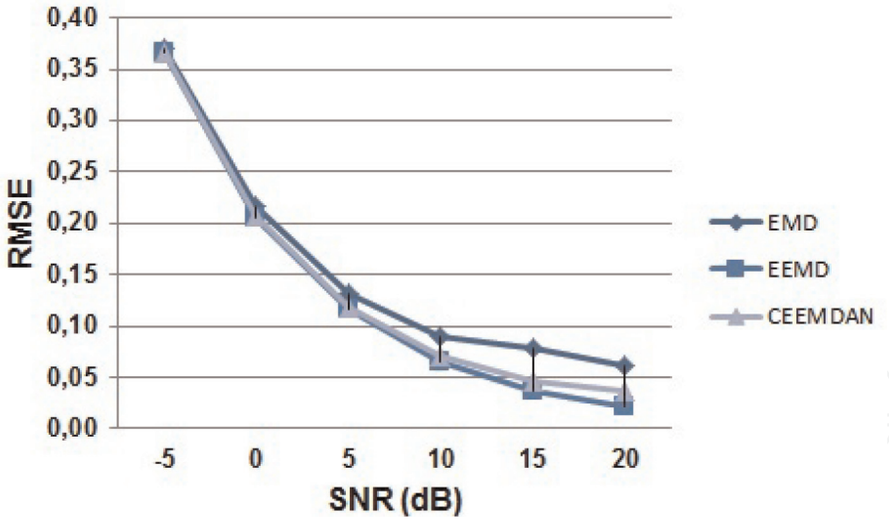

Figure 10.
RMSE comparison of the three denoising methods at different SNR levels for the supraventricular arrhythmia ECG signal.

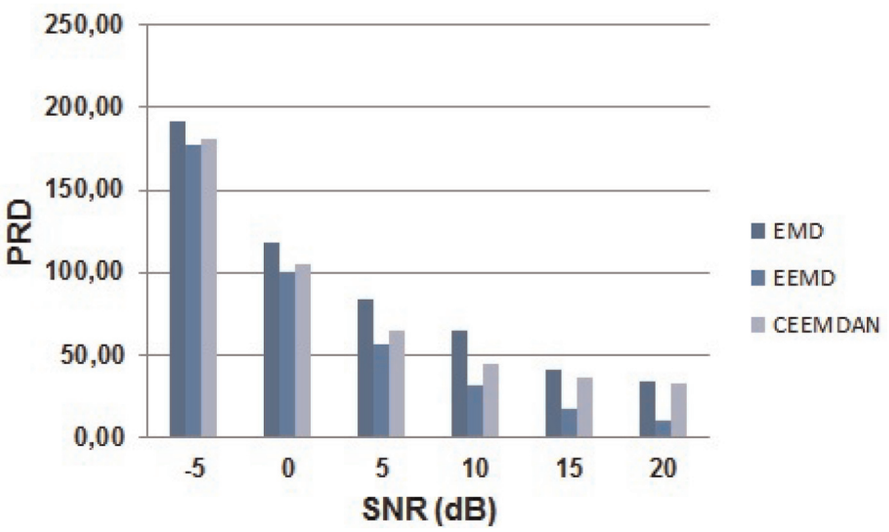

Figure 11.
PRD comparison of the different denoising methods at different SNR levels for the normal ECG signal.

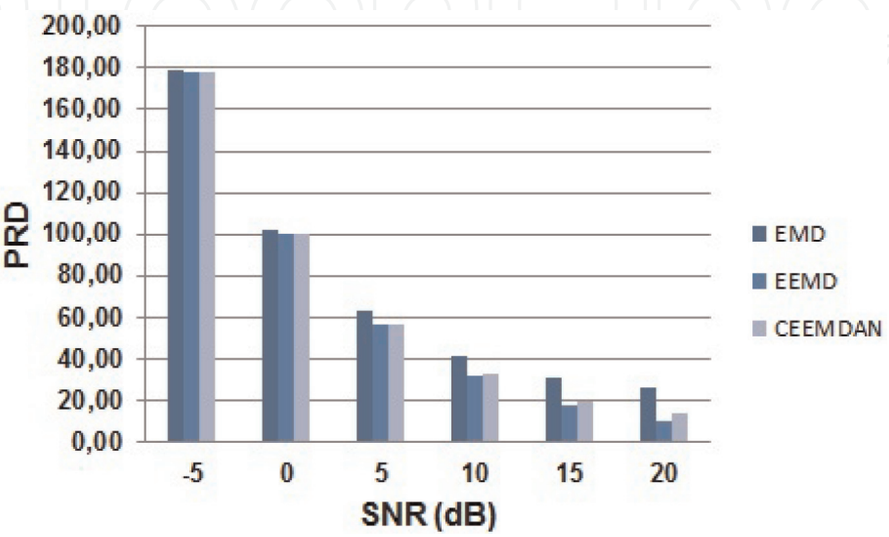

Figure 12.
PRD comparison of the different denoising methods at different SNR levels for the atrial fibrillation ECG signal.

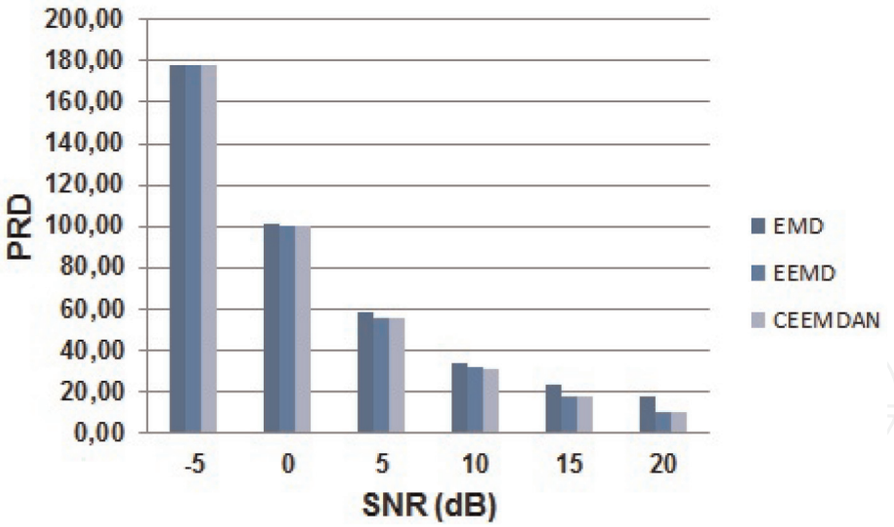

Figure 13.
PRD comparison of the different denoising methods at different SNR levels for the ventricular tachyarrhythmia ECG signal.

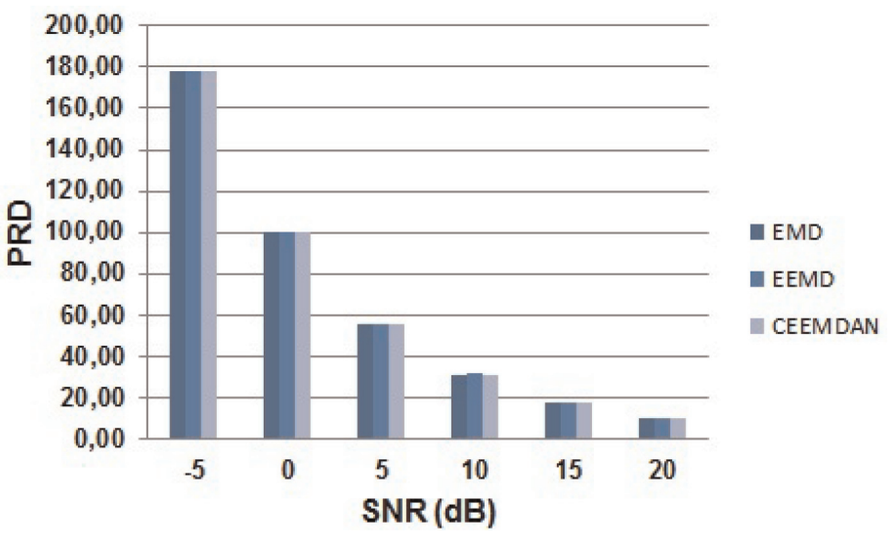

Figure 14.
PRD comparison of the different denoising methods at different SNR levels for the malignant ventricular arrhythmia ECG signal.

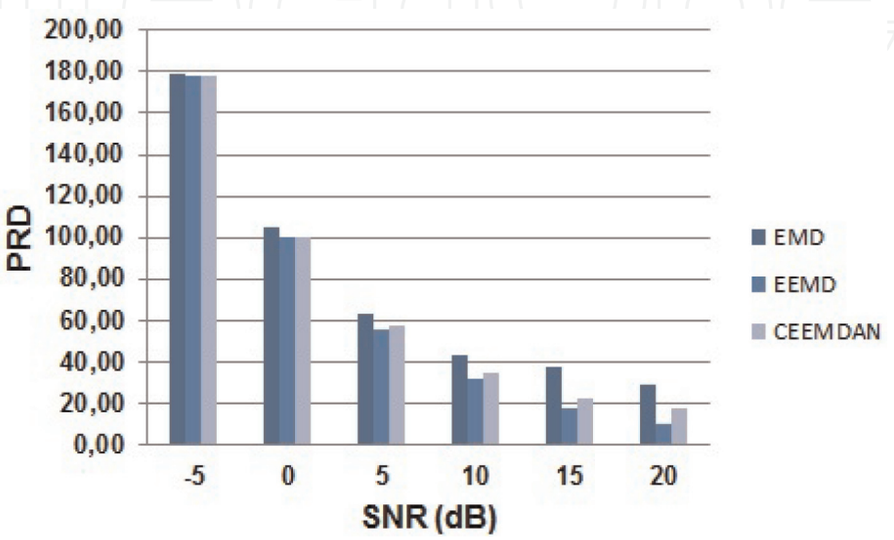

Figure 15.
PRD comparison of the different denoising methods at different SNR levels for the supraventricular arrhythmia ECG signal.

Section 2.3. Before applying the time-frequency techniques, these ECG signals were corrupted with different values of signal-to-noise ratio, varying from −5 to 20 dB with a 5 dB step.

Tables 6–10 report the obtained results of the mean square error (MSE), the root mean square error (RMSE), and the percent root mean square difference (PRD) after applying the three time-frequency methods (CW, PE, and SPWV) to the ECG signals, normal ECG, atrial fibrillation ECG, ventricular tachyarrhythmia ECG, malignant ventricular arrhythmia ECG, and supraventricular arrhythmia ECG, respectively.

SNR	Choi-Williams			Periodogram			SPWV		
	MSE	RMSE	PRD	MSE	RMSE	PRD	MSE	RMSE	PRD
−5	14.590	3.820	768.692	0.243	0.493	566.139	14.084	3.753	787.649
0	2.247	1.499	338.207	0.029	0.171	254.753	1.910	1.382	332.290
5	0.470	0.686	160.505	0.004	0.067	123.148	0.367	0.606	158.078
10	0.124	0.352	80.891	0.001	0.030	62.893	0.092	0.303	79.802
15	0.037	0.192	42.531	0.0002	0.015	33.357	0.027	0.163	42.003
20	0.011	0.106	22.983	0.0001	0.008	18.122	0.008	0.090	22.712

Table 6.
MSE, RMSE, and PRD of the normal ECG signal.

SNR	Choi-Williams			Periodogram			SPWV		
	MSE	RMSE	PRD	MSE	RMSE	PRD	MSE	RMSE	PRD
−5	13.303	3.647	271.222	0.252	0.502	151.833	13.340	3.652	270.031
0	2.270	1.507	131.224	0.041	0.202	75.307	2.202	1.484	126.352
5	0.478	0.691	67.090	0.008	0.090	39.165	0.458	0.676	64.774
10	0.119	0.345	35.616	0.002	0.044	21.018	0.113	0.335	34.446
15	0.033	0.181	19.362	0.001	0.023	11.501	0.031	0.176	18.746
20	0.010	0.098	10.678	0.0001	0.012	6.367	0.009	0.095	10.345

Table 7.
MSE, RMSE, and PRD of the atrial fibrillation ECG signal.

SNR	Choi-Williams			Periodogram			SPWV		
	MSE	RMSE	PRD	MSE	RMSE	PRD	MSE	RMSE	PRD
−5	65.469	8.091	423.064	1.295	1.138	220.730	65.501	8.093	418.365
0	11.304	3.362	196.830	0.222	0.471	105.949	11.196	3.346	188.372
5	2.351	1.533	97.777	0.046	0.213	53.838	2.327	1.526	93.922
10	0.571	0.756	50.923	0.011	0.105	28.461	0.565	0.751	49.037
15	0.154	0.393	27.357	0.003	0.054	15.431	0.153	0.391	26.384
20	0.045	0.211	14.981	0.001	0.029	8.496	0.044	0.210	14.461

Table 8.
MSE, RMSE, and PRD of the ventricular tachyarrhythmia ECG signal.

Figures 16–20 illustrate the RMSE comparison results obtained by using the different time-frequency techniques (CW, PE, and SPWV), at a SNR interval varying from −5 to 20 dB, to the following signals, respectively: normal ECG, atrial fibrillation ECG, ventricular tachyarrhythmia ECG, malignant ventricular arrhythmia ECG, and supraventricular arrhythmia ECG.

Figures 21–25 show the comparison PRD results of the three time-frequency techniques (CW, PE, and SPWV) to the five selected ECG signals.

SNR	Choi-Williams			Periodogram			SPWV		
	MSE	RMSE	PRD	MSE	RMSE	PRD	MSE	RMSE	PRD
−5	25.422	5.042	81.102	0.505	0.710	44.366	25.435	5.043	79.304
0	4.654	2.157	42.667	0.092	0.303	23.665	4.621	2.150	40.959
5	1.020	1.010	23.067	0.020	0.141	12.902	1.013	1.006	22.176
10	0.257	0.507	12.679	0.005	0.071	7.127	0.255	0.505	12.200
15	0.071	0.267	7.038	0.001	0.037	3.967	0.071	0.266	6.775
20	0.021	0.145	3.929	0.0004	0.020	2.218	0.021	0.144	3.783

Table 9.
MSE, RMSE, and PRD of the malignant ventricular arrhythmia ECG signal.

SNR	Choi-Williams			Periodogram			SPWV		
	MSE	RMSE	PRD	MSE	RMSE	PRD	MSE	RMSE	PRD
−5	0.410	0.640	1496.14	0.008	0.087	1300.33	0.407	0.638	1562.32
0	0.071	0.267	618.458	0.001	0.035	541.681	0.068	0.262	618.646
5	0.015	0.124	277.450	0.0002	0.016	244.693	0.015	0.121	277.768
10	0.004	0.062	133.833	0.0001	0.008	118.663	0.004	0.060	134.056
15	0.001	0.033	68.259	$2\ 10^{-5}$	0.004	60.743	0.001	0.032	68.391
20	0.0003	0.018	36.175	$5\ 10^{-6}$	0.002	32.266	0.0003	0.017	36.250

Table 10.
MSE, RMSE, and PRD of the supraventricular arrhythmia ECG signal.

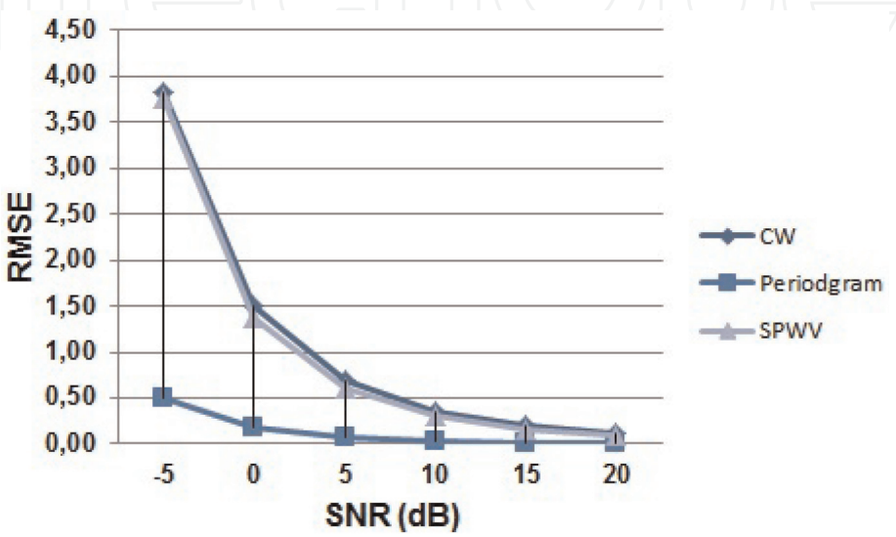

Figure 16.
RMSE comparison of the three time-frequency methods at different SNR levels for the normal ECG signal.

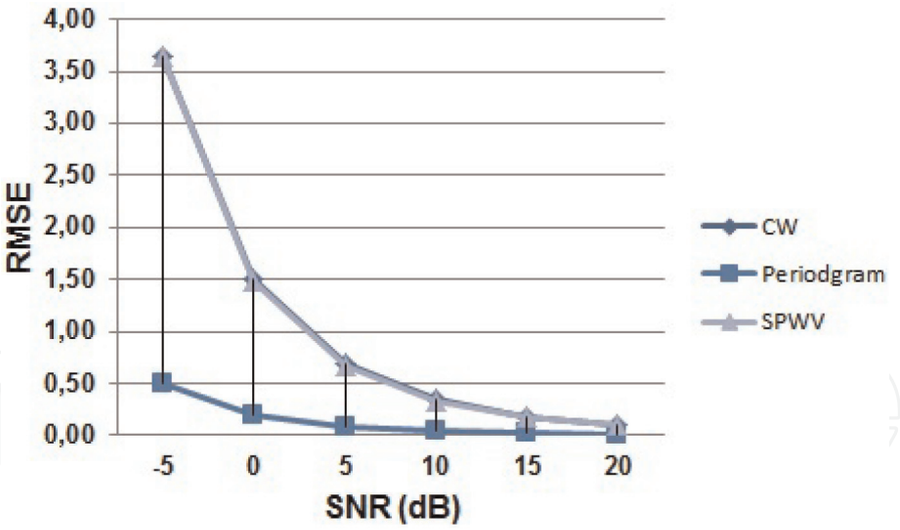

Figure 17.
RMSE comparison of the three time-frequency methods at different SNR levels for the atrial fibrillation ECG signal.

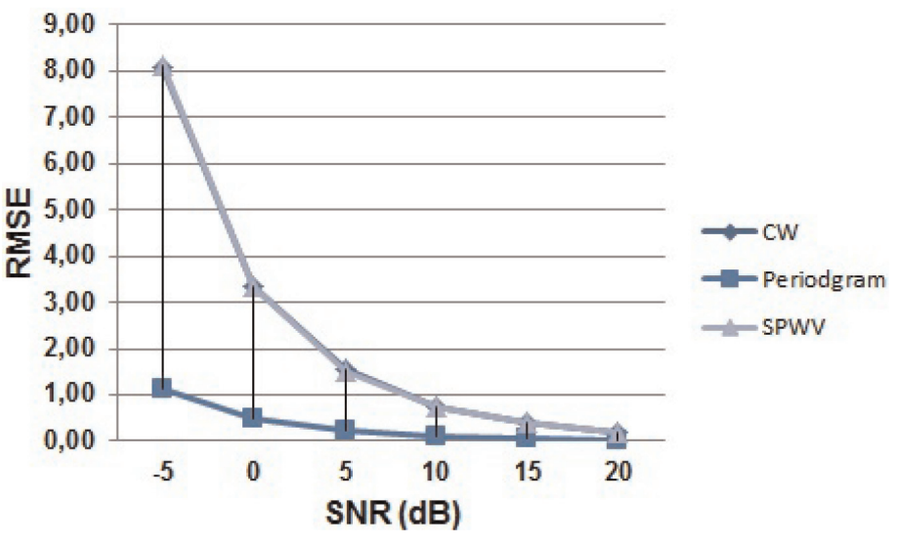

Figure 18.
RMSE comparison of the three time-frequency methods at different SNR levels for the ventricular tachyarrhythmia ECG signal.

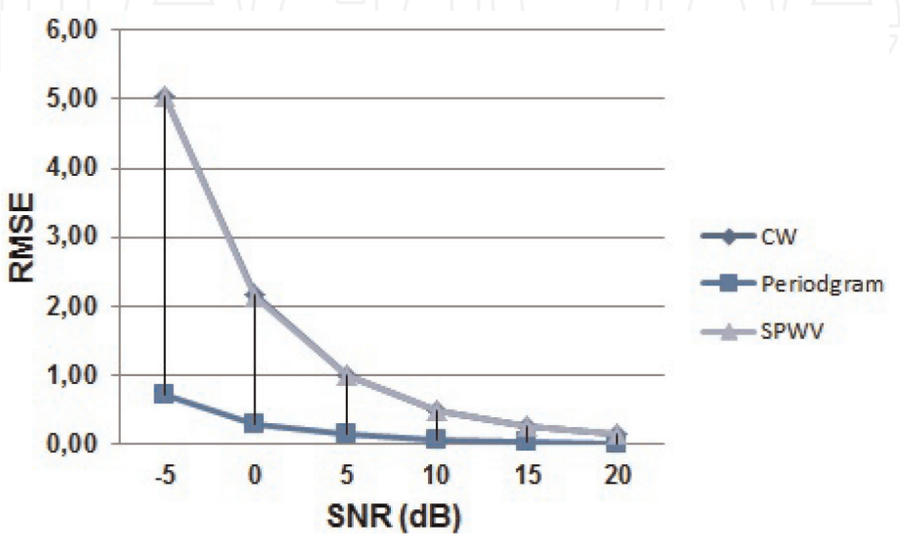

Figure 19.
RMSE comparison of the three time-frequency methods at different SNR levels for the malignant ventricular arrhythmia ECG signal.

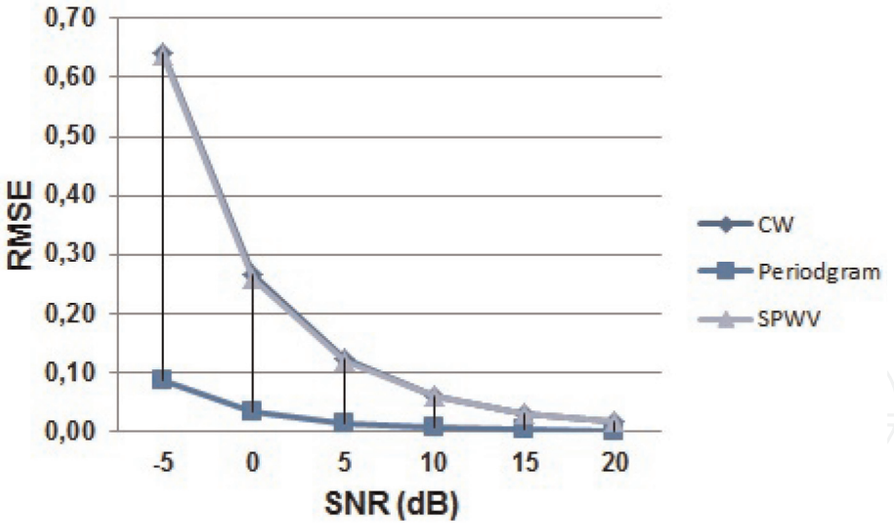

Figure 20.
RMSE comparison of the three time-frequency methods at different SNR levels for the supraventricular arrhythmia ECG signal.

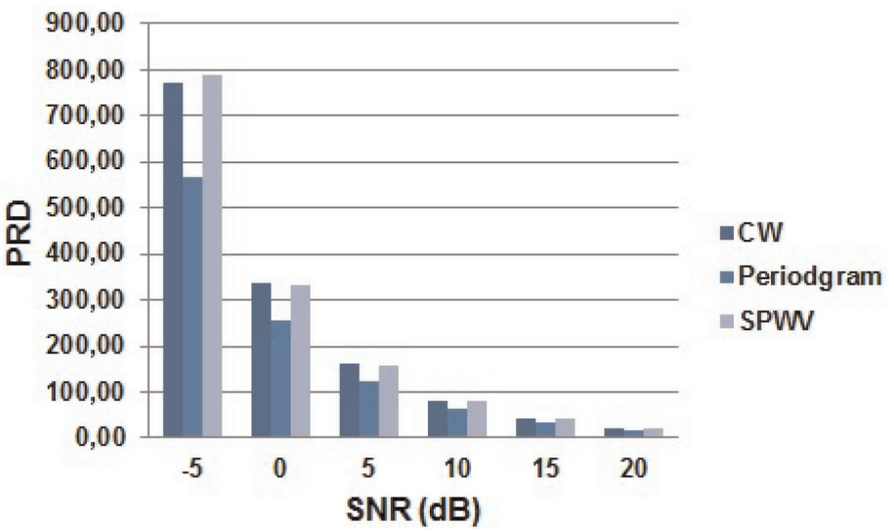

Figure 21.
PRD comparison of the three time-frequency techniques (CW, PE, and SPWV) at different SNR levels for the normal ECG signal.

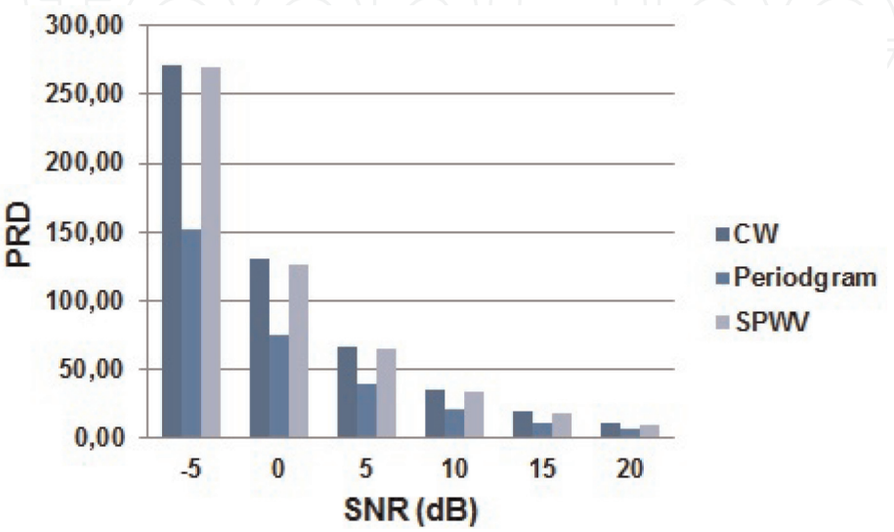

Figure 22.
PRD comparison of the three time-frequency techniques (CW, PE, and SPWV) at different SNR levels for the atrial fibrillation ECG signal.

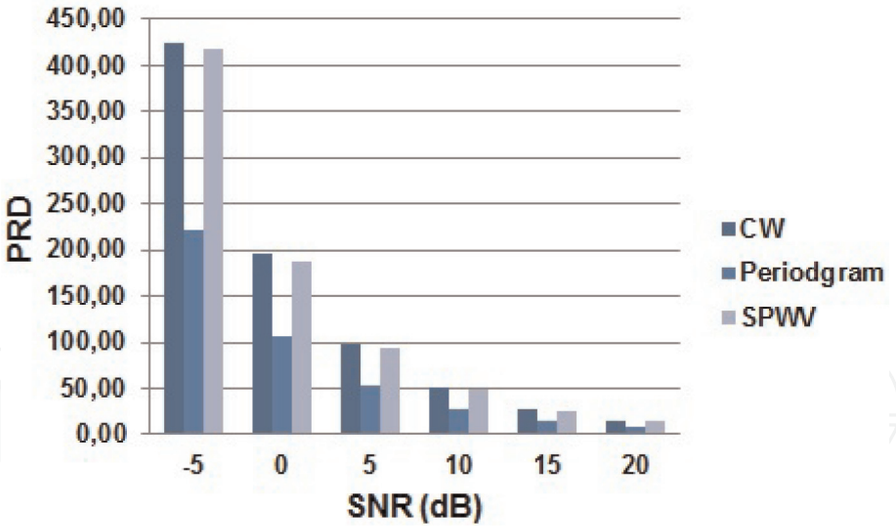

Figure 23.
PRD comparison of the three time-frequency techniques (CW, PE, and SPWV) at different SNR levels for the ventricular tachyarrhythmia ECG signal.

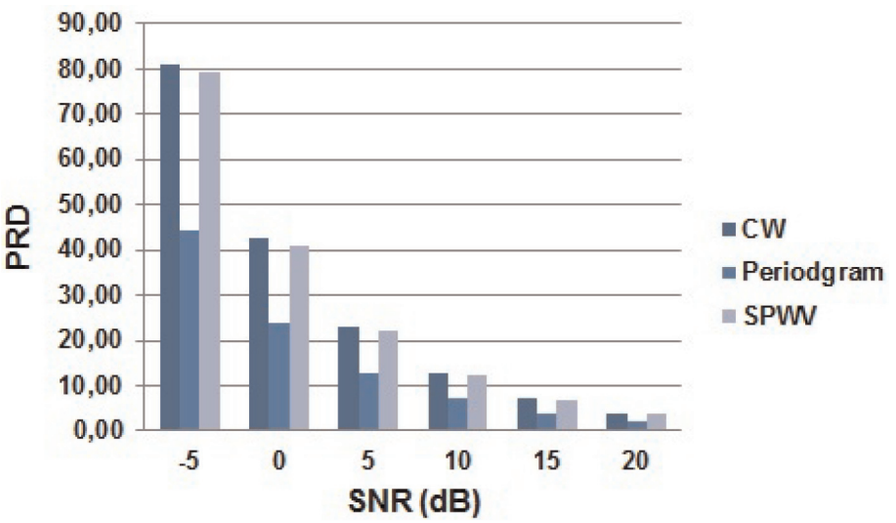

Figure 24.
PRD comparison of the three time-frequency techniques (CW, PE, and SPWV) at different SNR levels for the malignant ventricular arrhythmia ECG signal.

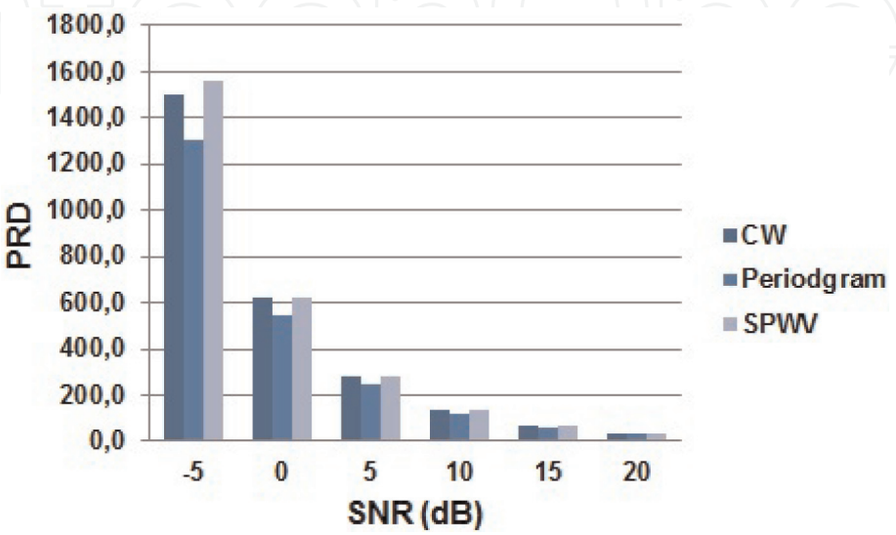

Figure 25.
PRD comparison of the three time-frequency techniques (CW, PE, and SPWV) at different SNR levels for the supraventricular arrhythmia ECG signal.

3.3 Discussion

The study was divided to two separate steps. The first part involved a comparison between three denoising methods, empirical mode decomposition (EMD) and its two variants ensemble empirical mode decomposition (EEMD) and complete ensemble empirical mode decomposition with adaptive noise (CEEMDAN). We note from the obtained results (**Tables 1–5** and **Figures 6–15**) that the EEMD and the CEEMDAN methods for the most selected ECG signals for the different signal-to-noise ratio (SNR) values yield the smallest values of MSE, RMSE, and PRD compared to those obtained by the EMD method. Despite the EEMD method providing a slight advantage than CEEMDAN for a few degrees of SNR in some ECG signals, we concluded that the most optimal technique for denoising this type of biomedical signals is CEEMDAN, especially for the large number of iterations required in EEMD process.

The second part of study presents a comparison of the different results of the three time-frequency techniques Choi-Williams (CW), periodogram (PE), and smoothed pseudo Wigner-Ville (SPWV). These time-frequency techniques were applied to normal and abnormal ECG signals with different degrees of SNR varying from −5 dB to 20 dB. We note that the PE technique provides the best results; it furnishes the smallest values of MSE, RMSE, and PRD than those obtained by the two other techniques, CW and SPWV.

After these two steps, we concluded that a combination of the two techniques, CEEMDAN denoising method and PE time-frequency technique, would be ideal for the ECG signal analysis. The CEEMDAN method will be reserved for the pre-treatment phase to filter the noise, and in the second phase, the PE technique will be applied to supply the evolution of the ECG signal fequential components over the time in order to provide a good diagnosis.

4. Conclusion

The work purpose was to conduct two comparative studies to determine the best techniques for ECG signal processing. The first one focused on the comparison between techniques aimed at preprocessing ECG signals, namely, denoising methods. The second one was to compare some time-frequency techniques that are intended to analyze these biomedical signals. The obtained results show that, in the first part, the CEEMDAN presents a high effectiveness in the noise elimination and, in the second one, the periodogram provides the best solution for analyzing ECG signals. We conclude that a combination of the CEEMDAN denoising method and the PE time-frequency technique can be a good issue in analyzing the ECG signals.

DOI: http://dx.doi.org/10.5772/intechopen.86007

Author details

Azzedine Dliou*, Samir Elouaham, Rachid Latif and Mostafa Laaboubi
ESSI-LISTI Laboratory, National School of Applied Sciences, Ibn Zohr University, Agadir, Morocco

*Address all correspondence to: dliou.azzedine@yahoo.fr

References

[1] Jones SA. ECG Success Exercises in ECG Interpretation. Philadelphia: F. A. Davis Company; 2008

[2] Clifford GD, Azuaje F, McSharry PE. Advanced Methods and Tools for ECG Data Analysis. Norwood: Artech House, Inc; 2006

[3] Sende J. Guide Pratique ECG. ESTEM ed; 2003

[4] El B'charri O, Latif R, Elmansouri K, Abenaou A, Jenkal W. ECG signal performance de-noising assessment based on threshold tuning of dual-tree wavelet transform. Biomedical Engineering Online. 2017;**16**(1):26

[5] Huang NE, Shen Z, Long SR, Wu MC, Shih EH, Zheng Q, et al. The empirical mode decomposition method and the Hilbert spectrum for non-stationary time series analysis. Proceedings Royal Society of London. 1998;**454A**:903-995

[6] Liao A-H, Shen C-C, Li P-C. Contrast improvement by combining pulse inversion with EMD and EEMD. In: Proceedings of the IEEE International Ultrasonics Symposium (IUS'09); Rome, Italy. 2009. pp. 287-290

[7] Torres ME, Colominas MA, Schlotthauer G, Flandrin P. A complete ensemble empirical mode decomposition with adaptive noise. In: Proceedings of the 36th IEEE International Conference on Acoustics, Speech, and Signal Processing (ICASSP'11). Prague, Czech Republic: IEEE; 2011. pp. 4144-4147

[8] Bigan C, Woolfson MS. Time–frequency analysis of short segments of biomedical data. IEE Proceedings Science, Measurement & Technology. 2000;**147**(6):368-373

[9] Clayton RH, Murray A. Estimation of the ECG signal spectrum during ventricular fibrillation using the fast Fourier transform and maximum entropy methods. In: Proceedings of the Computers in Cardiology. 1993. pp. 867-870

[10] Cooley JW, Tukey JW. An algorithm for machine calculation of complex Fourier series. Mathematics of Computation. 1965;**19**:297-301

[11] Addison PS. Wavelet transforms and the ECG: A review. Physiological Measurement. 2005;**26**:R155-R199

[12] Mousa A, Saleem R. Using reduced interference distribution to analyze abnormal cardiac signal. Journal of Electrical Engineering. 2011;**62**(3): 168-172

[13] Dliou A, Latif R, Laaboubi M, Maoulainine FMR. Abnormal ECG signals analysis using non-parametric time-frequency techniques. February 2014;**39**(2):913-921

[14] Latif R, Laaboubi M, Aassif E, Maze G. Détermination de l'épaisseur d'un tube élastique à partir de l'analyse temps-fréquence de Wigner–Ville. Journal of Acta Acustica. 2009;**95**(5): 843-848

[15] Hussain ZM, Boashash B. IF estimation for multicomponent signals. In: Time-Frequency Signal Analysis and Processing: A Comprehensive Reference. Oxford: Elsevier; 2003. pp. 437-445

[16] Cohen L. Time-frequency distributions—A review. Proceedings of the IEEE. 1989;**77**(7):941-981

[17] Cohen L. Time-Frequency Analysis. Englewood Cliffs: Prentice Hall PTR; 1995

[18] Flandrin P. Time-Frequency/Time-Scale Analysis. Boston: Academic Press; 1998

[19] Physiobank, Physionet. Physiologic Signal Archives for Biomedical Research. 2005. Available from: http://www.physionet.org/physiobank/ [Accessed: August, 2005]

[20] Elouaham S, Latif R, Nassiri B, Dliou A, Laaboubi M, Maoulainine F. Analysis electrocardiogram signal using ensemble empirical mode decomposition and time-frequency techniques. International Journal of Computer Engineering and Technology. 2013;**4**(2):275-289

[21] Flandrin P, Rilling G, Goncalves P. Empirical mode decomposition as a filter bank. IEEE Signal Processing Letters. 2004;**11**:112-114

[22] He X, Goubran RA, Liu XP. Ensemble empirical mode decomposition and adaptive filtering for ECG signal enhancement. In: Proceedings of 2012 IEEE International Symposium on Medical Measurements and Applications (MeMeA); 18-19 May 2012; Budapest, Hungary. 2012. pp. 1-5

[23] Yeh J-R, Shieh J-S, Huang NE. Complementary ensemble empirical mode decomposition: A novel noise enhanced data analysis method. Advances in Adaptive Data Analysis. 2010;**2**:135-156

[24] Colominas MA, Schlotthauer G, Torres ME. Improved complete ensemble EMD: A suitable tool for biomedical signal processing. Biomedical Signal Processing and Control. 2014;**14**:19-29

[25] Choi H, Williams W. Improved time-frequency representation of multicomponent signals using exponential kernels. IEEE Transactions on Signal Processing. 1989;**37**(6): 862-871

[26] Elouaham S, Latif R, Nassiri B, Dliou A, Laaboubi M, Maoulainine F. Analysis electroencephalogram signals using ANFIS and periodogram techniques. International Review on Computers and Software. 2013;**8**(12): 2959-2966